The role of electron-scale turbulence in the JET tokamak: experiments and modelling

P.Mantica[1], N.Bonanomi[2], A.Mariani[1], P.Carvalho[3], E.Delabie[4], J.Garcia[5], N.Hawkes[6], T.Johnson[7], D.Keeling[6], M.Sertoli[6], G. M. Staebler[8], G.Szepesi[6], D.Taylor[6], A. Thorman[6] and JET contributors*

[1]Istituto per la Scienza e Tecnologia dei Plasmi, CNR, via Cozzi 53, 20125 Milan, Italy
[2]Max-Planck-Institut für Plasmaphysik, D-85748 Garching, Germany
[3]Instituto de Plasmas e Fusão Nuclear, IST, 1049-001 Lisboa, Portugal
[4]Oak Ridge National Laboratory, Oak Ridge, TN 37831-6304, USA
[5]CEA, IRFM, F-13108 Saint-Paul-lez-Durance, France
[6]CCFE, Culham Science Centre, Abingdon, OX14 3DB, UK
[7]KTH Royal Institute of Technology, Stockholm, Sweden
[8]General Atomics, San Diego, CA 92186-5608, United States of America

E-mail: paola.mantica@istp.cnr.it

Abstract
Dedicated electron heat transport experiments have been carried out in L- and H-mode Deuterium plasmas of the JET-ILW tokamak to identify the amount of electron heat carried by electron-scale Electron Temperature Gradient (ETG) modes. Ion Cyclotron Resonance Heating at different positions has been used to probe the response of the electron temperature inverse gradient length R/L_{Te} to changes in electron heat flux q_e, whilst different amounts of Neutral Beam Heating allowed to scan the ratio of ion to electron temperature T_e/T_i, which is a key parameter for the onset of ETGs. Results indicate a steepening of the normalized q_e vs R/L_{Te} curve above R/L_{Te}~8 for $T_e/T_i \leq 1$, suggestive of the ETG onset. Ion-scale gyro-kinetic (GK) simulations match the ion heat flux and the low-R/L_{Te} part of the q_e curve, but do not reproduce such steepening at high R/L_{Te}. Multi-scale GK simulations covering both ion and electron scales and including one impurity bundling light and heavy species indicate an ETG contribution only for R/L_{Te} values larger than the experimental ones. Sensitivity studies of such result are difficult to achieve due to limitation in numerical resources. The quasi-linear TGLF model has been used for sensitivity studies. With the same bundled impurity as the GK multi-scale, TGLF shows the q_e steepening at much larger R/L_{Te} values than in experiment, but when using the real mix of light impurities neglecting the heavy impurities, TGLF gets closer to the experimental results. Profile simulations with TGLF including both light and heavy impurities show over-prediction of T_e profiles and in some cases also of density, but good T_i predictions, confirming issues with the model electron stiffness for these plasmas.

Keywords: turbulent transport, electron-scale turbulence, multi-scale interactions, gyrokinetic simulations, quasilinear simulations

1. Introduction

Electron heat transport will play a more strategic role in determining fusion power production in future reactors with dominant electron heating than it does in present devices with dominant ion heating. In fact in the electron heating case the ion temperature T_i can never exceed the electron temperature T_e (since the ion heating comes from the electron channel through collisional exchange) whilst in the ion heating case at low collisionality T_i can peak even if T_e is limited by turbulence. This has triggered a renewed effort to clarify the electron heat transport mechanisms and validate theoretical models for their description, for an increased reliability of predictive simulations.

Early studies of electron heat transport in small/medium size devices with dominant Electron Cyclotron Resonance Heating (ECRH) and $T_e/T_i >> 1$ (see [1] for a re-

* See the author list of 'Overview of JET results for optimising ITER operation' by J. Mailloux et al. to be published in Nuclear Fusion Special issue: Overview and Summary Papers from the 28th Fusion Energy Conference (Nice, France, 10-15 May 2021)

view) had validated a picture of electron heat transport due to ion-scale turbulence, i.e. Ion Temperature Gradient (ITG) and Trapped Electron Modes (TEM), the latter characterized by mild levels of stiffness (i.e. the response of the turbulent normalized electron heat flux q_e to the electron temperature inverse gradient length $R/L_{Te}=R|\nabla T_e/T_e|$ with R the major radius). However recent studies in several devices in presence of mixed ion and electron heating with $T_e/T_i \leq 1$ and with high R/L_{Te} drive have revealed high levels of electron stiffness, that ion-scale gyrokinetic (GK) simulations are unable to match [2-7]. These are experimental indications of a possible role of electron scale instabilities, i.e. Electron Temperature Gradient (ETG) modes, whose linear threshold is known to scale with Z_{eff} T_e/T_i [8], where $Z_{eff} = \frac{\sum_i z_i^2 n_i}{n_e}$. Modelling ETG transport requires nonlinear multi-scale GK simulations, covering both ion and electron scales and accounting for their coupling, since multi-scale interactions determine an effective nonlinear threshold for ETG transport gaining importance over the ion-scale instabilities. These simulations are computationally very heavy and only few have been performed so far with realistic mass ratio [3,4,9,10]. They indicate that indeed in such situations a significant fraction of electron heat is driven by ETGs. However in some cases due to limits in computational resources some approximations were made, e.g, in the cases of JET [4] and AUG [10] impurities were neglected, thereby making the comparison with experiment only qualitative. In addition, experimentally it is not easy to have clear-cut evidence of electron heat fluxes not accounted for by ion-scale turbulence, due to uncertainties in the T_i, T_e, n_e gradients and in the heat depositions. It is also difficult to push the normalized q_e very high above the ETG threshold, e.g. in the TCV [6] and AUG [7] experiments the q_e was very marginally above threshold and the main evidence for high stiffness came from the analysis of the T_e modulation, which allows an independent determination of the local slope of the q_e vs R/L_{Te} curve.

For these reasons, new experiments have been performed at JET, using different NBI levels to scan T_e/T_i and using ICRH on- vs off-axis to scan the q_e vs R/L_{Te} curve. These data have then been addressed by ion-scale and multi-scale GK simulations including also impurities. The quasi-linear model TGLF both in its "SAT1-geo" version [11,12] and in its very recent "SAT2" version [12] has also been compared with experiments and with GK, to validate its ability to properly predict multi-scale transport.

Sect.2 described the experimental set-up, Sect.3 the experimental results, Sect.4 the ion-scale and multi-scale GK simulations, Sect.5 the TGLF tests, with Sect.6 summarizing the main conclusions and providing an outlook for future work.

2. Experimental set-up and results

Dedicated electron heat transport experiments have been performed in JET ILW (ITER-like-wall) (R/a=2.96m/0.95m) in Deuterium L- or H-mode plasmas with toroidal magnetic field $B_T \sim 3.3$ T, plasma current $I_p \sim 2$ MA, safety factor at the magnetic surface enclosing the 95% of the poloidal magnetic flux $q_{95} \sim 5$, electron density in the plasma center $n_{e,0} \sim 3$–4×10^{19} m^{-3}, and different levels of neutral beam injection (NBI) and ion cyclotron resonance heating (ICRH). Z_{eff} varies over the whole dataset between 1.5 and 2.8, depending sensitively on the ICRH power, bringing in metallic impurities. Be, C, Ni and W are intrinsic and Ne is injected in minimal amounts for charge-exchange measurements. Heavy impurities are the main contributors to the largest Z_{eff} values. In these discharges there is no significant MHD activity apart from sawteeth in the later phase of each discharge. However, due to high q_{95}, the inversion radius is small and they do not affect the region where we study ETGs. In these experiments, mid-radius q_e scans at constant total power were carried out by using on- versus off-axis ICRH power in different proportions in (H)– D plasmas with $n_H/n_e \sim 5\%$ to achieve dominant electron heating. These q_e scans allow to determine the R/L_{Te} threshold for the onset of turbulent electron heat transport and the electron stiffness, which we define as the slope of the gyro-Bohm normalized heat flux q_e^{GB} vs R/L_{Te} ($q_e^{GB} = q_e /(n_e T_e c_s \rho_s^2/R^2)$ with $c_s = \sqrt{T_e/m_i}$ and $\rho_s = m_i c_s/eB$, m_i being the ion (Deuterium) mass, e the electron charge and B the toroidal magnetic field). Unfortunately the use of H minority heating prevented the use of T_e modulation via ICRH modulation, due to too broad deposition profiles and too long fast ion slowing down times, unlike in [4] where the use of Mode Conversion allowed T_e modulation at the expenses of a higher Z_{eff} due to the high ^{3}He concentration needed. In the present experiments we privileged the need of a cleaner plasma to achieve a lower ETG threshold and facilitate their detection. The NBI power was varied between 0 and 20 MW, whilst the ICRH power was generally kept at 6 MW, with some shots at 3 MW. This allowed to obtain sets of q_e scans at different T_e/T_i. At the radius examined for the ETG detection, $\rho_{tor}=0.5$ with $\rho_{tor} = \sqrt{(\Phi/\pi B_T)}/\sqrt{(\Phi/\pi B_T)_{max}}$, T_e/T_i varied from 0.8 at high NBI to 1.3 at low NBI and full ICRH power. The central T_e/T_i variation was obviously much larger.

Figure 1 shows as an example the time traces of some main plasma parameters and powers, with two NBI levels explored in each shot to minimize the number of shots required to achieve a sufficient dataset.

Figure 2 shows as an example the radial profiles (averaged over typically 0.5-1 sec) of temperatures, density, toroidal rotation and safety factor (q) profile for a pair of shots with 6 MW of NBI power and on- vs off-axis 6 MW ICRH power. T_e is measured by high resolution Thomson Scattering (HRTS) and Electron Cyclotron Emission (ECE) radiometer, T_i and rotation are measured by Active Charge Exchange (CX) on Ne and D-α, n_e is measured by HRTS and LIDAR Thomson Scattering, q is reconstructed by EFIT [13] with constraints from magnetic measurements and pressure for the best reconstruction of magnetic surfaces used for diagnostic mapping, and with additional Faraday rotation constraint for a better reconstruction of the q profile in the inner region. The figure shows also the experimental error bars and the fits obtained by Gaussian Process Regression

(GPR) [14]. Errors on R/L_{Te} and R/L_{Ti} are estimated around ± 20%, for R/L_n around ±40%. We note a tendency of the q and n_e profile peaking to increase from off-axis to on-axis ICRH, which will be discussed later.

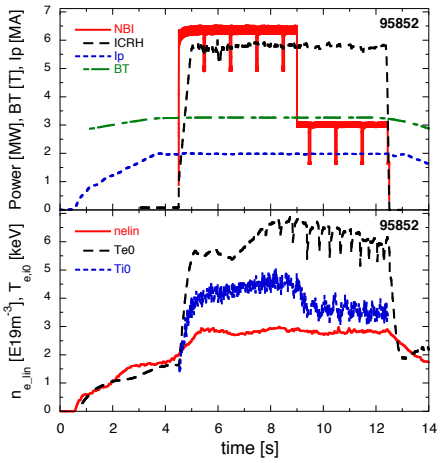

Figure 1. Time traces for shot 95852 of a) NBI and ICRH power, plasma current and toroidal field; b) line averaged electron density, central electron and ion temperatures. The NBI notches are on purpose for Charge Exchange diagnostics.

From the fitted profiles the values of R/L_{Te} and associated uncertainties are calculated, with the spatial derivatives taken with respect to the flux surface label $r = (R_{out} - R_{in})/2$, where R_{out} and R_{in} are the outer and inner boundaries of the flux surface on the magnetic axis plane. q_e at ρ_{tor}=0.5 is obtained by calculating the NBI power deposition with PENCIL [15], the ICRH deposition by PION [16], and in some cases by SELFO [17] as a cross-check, the radiated power from bolometry, the Ohmic power and collisional coupling are estimated with analytic formulae for resistivity and collision time and in some cases cross-checked with interpretative transport simulations using the ASTRA [18] transport code. This procedure leads to the q_e^{GB} vs R/L_{Te} plot shown in Figure 3a, where we show 3 sets of points, distinguishing the different NBI levels (<1.5 MW, 4.5-6 MW and 16-20 MW) and consequently the T_e/T_i value (respectively T_e/T_i at ρ_{tor}=0.5 ~1.3, 1, and 0.9). We note that in Figure 3 amongst the whole set of experimental points we have retained those presenting similar value of parameters such as q, s, s/q, R/L_n, R/L_{Ti}, Z_{eff}, T_e/T_i, since the q_e scan is ideally to be made varying R/L_{Te} at constant other parameters. More precisely, the maximum excursions for the set T_e/T_i =1, corresponding to pairs of fully on- vs off-axis, are: $4.5<R/L_{Ti}<5.8$, $1.85<R/L_n<2.6$, $1.76<q<2.18$, $0.47<s<0.87$, $0.22<s/q<0.49$, $1<T_e/T_i<1.18$. However it has to be noted that these are the real extremes comparing full on and off-axis, and many points that are on-axis with somewhat different total power or mixed on- and off-axis have much less variations. In fact, by isolating points with very similar parameters, we have cross-checked that the curve slope is consistent with the whole set. Z_{eff} is typically comprised between 1.8 and 2.2, but, being rather sensitive to the level of ICRH power, there are 2 discharges with very high ICRH that reach Z_{eff}=2.8, and 2 discharges at low ICRH that have Z_{eff}~1.5-1.7.

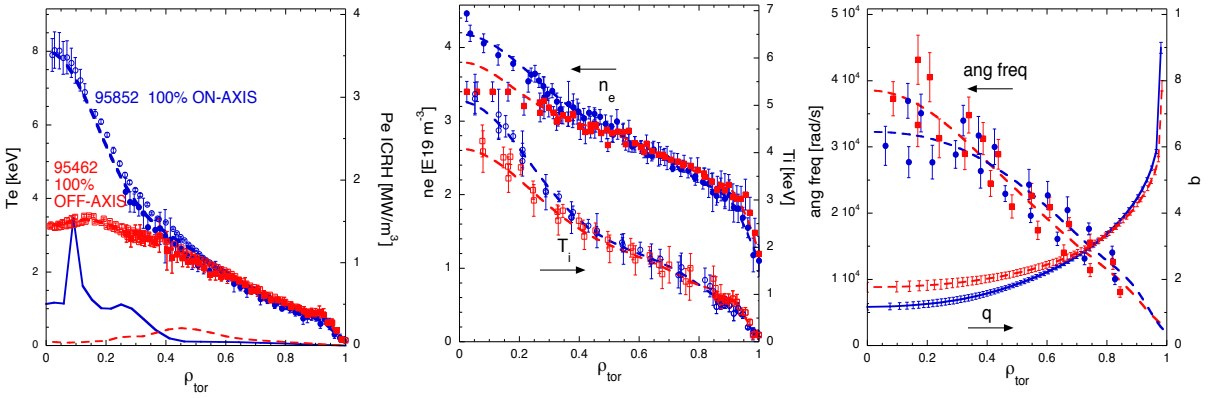

Figure 2. Radial profiles for a couple of shots with ON vs OFF axis ICRH, NBI power=6 MW: a) electron temperature b) electron density and ion temperature c) toroidal angular frequency and safety factor. Blue refers to on-axis (averaged around t=8 sec) and red to off-axis (averaged around t=6.5 sec). For T_e HRTS is full symbols and ECE radiometer is open symbols. Dashed lines are the GPR fits.

The high NBI points in Figure 3 (T_e/T_i ~0.9) are in H-mode with high pedestal, therefore the gyroBohm normalization over $n_eT_e^{5/2}$ pushes them to the low q_e^{GB} region, making impossible to have a stiffness estimate. Instead the two sets with low and medium NBI are in low pedestal H-mode and L-mode respectively, therefore a good scan of q_e^{GB} values could be achieved. To the extent that the minor differences in parameters can be neglected, these two sets of data allow to determine a threshold and a slope indicating the stiffness level, which we define as $\partial q_e^{GB} / \partial R/L_{Te}$. We note that a scan in normalized ion heat flux q_i^{GB} is also produced as a side effect, as shown in Fig.3b. This indicates very high ion stiffness for the 3 sets. This property will be used to adjust the q_i^{GB} match of simulations in Sect.3 and 4, by small variations of R/L_{Ti} within error bars. Matching q_i^{GB} is in fact very important for the non-linear ETG dynamics. Concerning the variation in q and n_e peaking observed when going from off-axis to on-axis ICRH (R/L_n: 1.85→2.6, q:2.18→1.76, s:0.47→0.87, s/q:0.22→0.49) we note that they basically cancel out in the TEM threshold expression given in [19]:

$$\frac{R}{L_{Te}}^{TEM} = \frac{0.357\sqrt{\epsilon} + 0.271}{\sqrt{\epsilon}}\left[4.9 - 1.31\frac{R}{L_n} + 2.68s + ln\left(1 + 20\nu_{eff}\right)\right] \quad (1)$$

where ε is the local aspect ratio and ν_{eff} the effective collisionality, so they would not alter the part of the experimental curve at lower flux (q_e^{GB} <40) which is expected dominated by TEMs. This is in fact confirmed by the fact that shot 95461, which is on-axis but had a bit larger power level, ends up very near to the off-axis 95462. Instead on the ETG threshold expressed by [8]:

$$\left(\frac{R}{L_{Te}}\right)^{ETG} = max\left[\left(1+z_{eff}\frac{T_e}{T_i}\right)\left(1.33 + 1.91\frac{s}{q}\right), 0.8\,\frac{R}{L_n}\right] \qquad (2)$$

(where at experimental R/L_n it is the first term that matters) the change in s/q determines an increase in threshold of R/L_{Te} ~0.5 for the on-axis case, so that it does not fall on exactly the same curve as the off-axis point. This implies that the apparent stiffness when fitting both points with the same curve is a lower limit to the real stiffness, in case ETGs start playing a role.

Overall the three sets of points have similar threshold within experimental uncertainties, thus independent of T_e/T_i. We remark that the flat q_e^{GB} values at low R/L_{Te} for the T_e/T_i =1.3 set are typically indicative of the q_e bias due to ITGs and do not indicate a lower threshold. Such independence of threshold from T_e/T_i points to that being the TEM threshold, since ETGs are predicted to have a stronger T_e/T_i dependence. The stiffness of the two sets at medium and low NBI is also similar in the region q_e^{GB} <40, and shows signs of higher stiffness for the T_e/T_i ~1 set above q_e^{GB} =40, although the number of points is low. The highest points were reached by lowering a bit the total power besides having fully on-axis ICRH, but still preserving similar parameters, with a bit lower Z_{eff}. Given the difficulty in achieving high q_e^{GB} points and their importance for our ETG assessment, these points were carefully validated by comparing different fitting techniques to calculate the profile gradients and using both PION and SELFO for ICRH deposition, which we found in very good agreement. The question that will be investigated in the following sections is then whether such apparent increase of stiffness may be linked with the onset of ETGs, which have a lower threshold at T_e/T_i ~1 with respect to T_e/T_i~1.3.

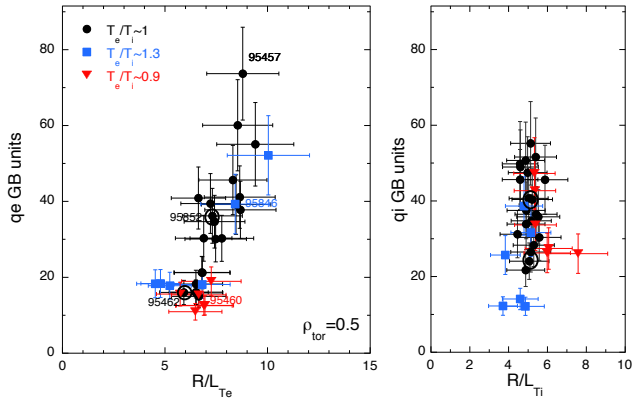

Figure 3. Normalized electron and ion heat fluxes at ρ_{tor}=0.5 vs R/L_T for different T_e/T_i. The two encircled shots 95852 and 95462 are the on-off-axis pair of Fig.2. The 3 shots 95457, 95846, 95460 are examples from the 3 sets targeted by TGLF simulations in Sect.4.2.

3. Gyrokinetic simulations

Starting from the experimental parameters of JET discharge #95457 at t = 9.25s and at ρ_{tor}=0.5, gyro-kinetic simulations with the GENE [20,21] code have been performed.

3.1 Simulations set-up

The values of the main parameters used in the simulations are: R/L_{Te} = 9, R/L_{Ti} = 5.77 when not otherwise stated, R/L_n = 3.1, s=1.02, q=1.8, T_e/T_i = 1, Z_{eff} = 1.5. We note that with these parameters the linear ETG threshold given by Eq.(2) is R/L_{Te}~6. GENE solves the gyro-kinetic Vlasov equations [22] coupled with the Maxwell equations within a δf approximation and using a set of field aligned coordinates $\{x, y, z, v_\parallel, \mu\}$. z is the coordinate along the magnetic field line, x is the radial coordinate, y is the binormal coordinate, $v_\parallel$, is the parallel velocity and μ is the magnetic moment. The simulations are carried out in the local limit and using realistic geometry (reconstructed from numerical equilibrium files provided by the EFIT equilibrium solver), collisions (using a Landau-Boltzmann collisional operator), finite β_e effects (considering only $B_\perp$ fluctuations), kinetic ions, electrons and one impurity species (C) with concentration 1.7%, devised to lump together all impurities reproducing the experimental Z_{eff} and ion dilution. In the real experiment these are due to Be (1%), C (0.1%), Ne (0.15%), Ni (0.064%) and W (0.0055%), as measured by a constrained multi-diagnostic analysis [23] and by Charge Exchange. This shot in the chosen time interval had negligible rotation (only NBI blips for CX measurements), so no ExB or Parallel Velocity Gradient terms have been included in the GK simulations. Also the fast ion content at ρ_{tor}=0.5 is negligible. Both ion-scale $(0 < k_y\rho_s < 1.2)$ and multi-scale $(0 < k_y\rho_s < 30)$ simulations are carried out in order to study the role of ETGs ($k_y\rho_s$ *is* the wave number in the binormal direction, normalized by ρ_s defined in Sect.2).

3.2 Linear multi-scale GK simulations

$k_y\rho_s$ scans of linear GENE simulations have been performed to characterize the micro-turbulence regimes at ion and electron scales. Reference parameters have been considered, using two values of R/L_{Ti} and varying R/L_{Te} from the nominal value 9 to 14. The linear simulations have been run with $[n_x, n_y, n_z, n_{v_\parallel}, n_\mu] = [48,1,32,32,12]$ points in the reduced 5-dimensional gyro-kinetic phase-space grid. The results are shown in figure 4, where the eigenvalues corresponding to the most unstable linear mode at each $k_y\rho_s$ are presented vs $k_y\rho_s$. In particular, the spectrum of the ratio γ/k_y of the growth rate γ divided by k_y, normalised with $\rho_s c_s/R$, is shown on the top, while the spectrum of the normalized mode angular frequency ω is shown on the bottom. At ion scales ITG modes are mainly found, except from the R/L_{Te}=14 case, where TEMs dominate. ETG modes are found at electron scales. Two separate ITG and ETG growth rate peaks are present for lower R/L_{Te}=9,11 cases, while a continuous TEM-ETG

branch links the two scales when R/L_{Te}=14. A simple criterion from [24] states that ETGs should impact the nonlinear electron heat fluxes if the ratio $(\gamma/k_y)_{max,ETG}/(\gamma/k_y)_{max,ITG}$ of the peaks at electron and ion scales in the linear γ/k_y spectrum becomes >1. According to this, a non-negligible contribution of ETGs to q_e is expected for $R/L_{Te} \geq 11$ for the case with R/L_{Ti}=5.77 and for $R/L_{Te} \geq 9$ for the case with R/L_{Ti}=5.17.

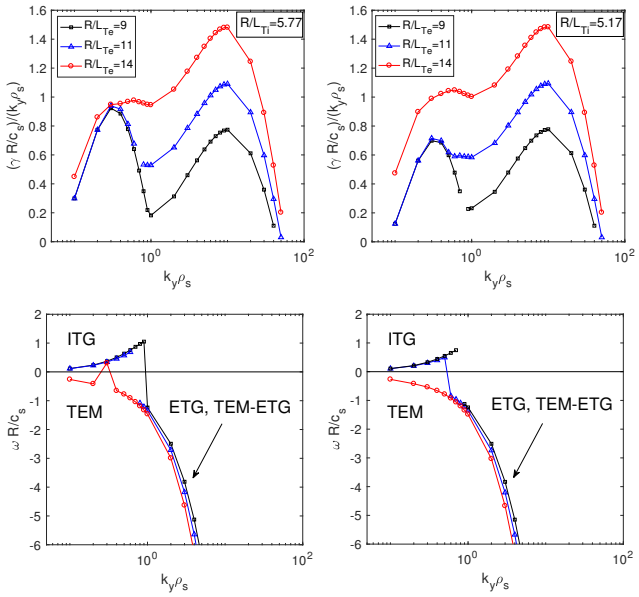

Figure 4. (top) k_y spectrum of $(\gamma R/c_s)/(k_y\rho_s)$; (bottom) k_y spectrum of $\omega R/c_s$ for the two cases R/L_{Ti}=5.77 (left) and R/L_{Ti}=5.17 (right), at 3 different R/L_{Te} values.

3.3 Nonlinear ion scale GK simulations

The ion-scale non-linear simulations have been performed using radial and binormal box sizes $[Lx, Ly] = [88.6,83.8]\rho_s$, corresponding to $k_{y,min}\rho_s = (2\pi/Ly)\rho_s = 0.075 \sim k_{x,min}\rho_s = (2\pi/Lx)\rho_s = 0.071$. The simulations have been run with $[n_x, n_y, n_z, n_{v_\parallel}, n_\mu] = [256,24,32,32,12]$ points in the reduced 5-dimensional gyro-kinetic phase-space grid. These values were chosen after dedicated convergence tests and for a direct comparison with the multi-scale simulation results.

The results from the ion scale simulations are shown in figure 5. The black circles represent the experimental data with T_e/T_i = 1, the bigger black circle being the data point from JET discharge #95457. Both the gyro-Bohm normalized electron and ion heat fluxes are shown. Three different values of R/L_{Ti} were used in the gyro-kinetic ion-scale simulations (R/L_{Ti} = 4.8, 5.77, 6) and scans in R/L_{Te} were performed for each value of R/L_{Ti}.

As visible for the right plot of Figure 5, the ion heat flux is very stiff in R/L_{Ti}, as ITGs are dominant in these cases. Changing RL_{Ti} has an impact also on the electron heat flux, with an increase of $q_{e,gB}$ of ~100% when changing R/L_{Ti} from 4.88 to 6. However, changing R/L_{Ti} does not impact the stiffness of the electron heat flux with respect to R/L_{Te}. For the RL_{Ti} =5.77 case, a study of the effect of R/L_n was also performed, increasing the nominal value of R/L_n by 40%. When increasing R/L_n the electron heat flux increases by about 40% (stronger TEM), while the ion heat flux decreases. This is visible comparing the blue and the light blue points in Figure 5. Also in this case, no strong effect on the electron heat flux stiffness with respect to R/L_{Te} was observed. Due to such lack of impact on electron stiffness of changes of R/L_{Ti} or R/L_n, it is evident that improving the match in q_e^{GB} values of the upper part of the graph by increasing R/L_{Ti} or R/L_n decreases the agreement with the lower part. From these results it appears that, while the single data point can be reproduced by changing within uncertainties the input parameters in the gyro-kinetic simulations, the experimental slope of the electron heat flux with respect to a change in R/L_{Te} is underestimated by the simulations. To match the slope, a mechanism providing a q_e contribution scaling with R/L_{Te} would be needed. We also observe that the choice of R/L_{Ti}=5.77 and nominal R/L_n matches well q_i^{GB} and the lower part of the q_e^{GB} curve, whilst the experimental value R/L_{Ti}=4.8 underestimates q_i heavily. Since for multiscale dynamics it is key to have the correct ion heat flux, the two values of R/L_{Ti}=5.77 and R/L_{Ti}-=5.17 (which provide q_i^{GB} values respectively at the upper and lower ends of the q_i^{GB} error bar) and the nominal values for all the other parameters have been chosen for the multiscale simulations described in the next section.

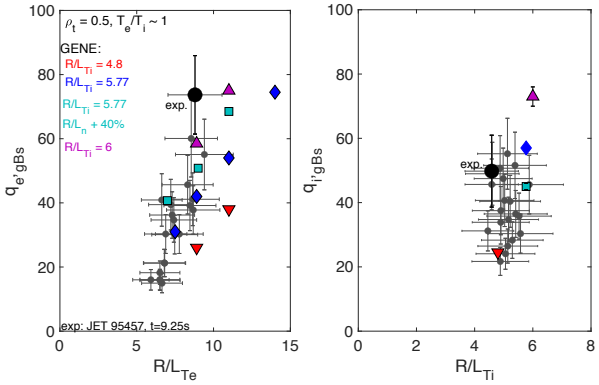

Figure 5. q_e^{GB} vs R/L_{Te} (left) and q_i^{GB} vs R/L_{Ti} (right) for the experimental shots with T_e/T_i=1 (black circles) and GENE non-linear ion-scale simulations with 3 values of R/L_{Ti} and one increased value of R/L_n, as in the legend.

3.2 Multi-scale GK simulations

Four nonlinear multi-scale gyrokinetic simulations have been run with the flux-tube version of the GENE code for R/L_{Te}=9,11,14 and R/L_{Ti} = 5.77 and for R/L_{Te}=11 and R/L_{Ti} = 5.17, to compare with the corresponding ion-scale results and single out the ETG contribution to the nonlinear fluxes. Each of these simulations has used ~ 10.3 Million CPU hours. The effect of the impurities, being responsible of an up-shift of the ETG linear R/L_{Te} threshold ~ $(1 + Z_{eff}T_e/T_i)$, has been taken into account considering a single effective species (C at 1.7% concentration) as in the single-scale runs. Electromagnetic effects and realistic EFIT geometry have been kept in the simulation. In order to reduce the computational effort of these very challenging simulations, the multi-scale simulation of the initial nonlinear saturation phase has been avoided for each run as follows. First, an ion-

scale simulation has been run for R/L_{Te}=9 with the same number of k_x modes needed for the corresponding multi-scale (1536). Then, after the nonlinear convergence of the fluxes, a checkpoint has been saved and the simulation has been restarted from it expanding the k_y grid up to $k_y\rho_s = 38.4$ to include electron scales, thus becoming a multi-scale. The radial and binormal box sizes have been set to the same values of the ion scale runs. The simulations have been run with $[n_x, n_y, n_z, n_{v_\parallel}, n_\mu] = [1536, 512, 32, 32, 12]$ grid points. The multi-scale runs at larger R/L_{Te}=11,14 have been initialised changing R/L_{Te} starting from checkpoints of R/L_{Te}=9,11 simulations, respectively, which showed saturated fluxes. An example of the time traces of the fluxes in gB units is shown in Figure 6 for the R/L_{Te}=14 case. For each R/L_{Te}, a $\Delta t \sim 40 - 50R/c_s$ statistics has been collected, corresponding to 2-3 'global' flux oscillations. A rough estimate of the numerical error bars that can be associated to the NL multi-scale fluxes is ± 5%, which corresponds to the typical standard deviation of the running average of the fluxes over the collected oscillations.

In Figure 7 the results of the multi-scale simulations (blue stars for R/L_{Ti}=5.77 and red stars for R/L_{Ti}=5.17) are compared with the corresponding ion-scale results (blue and red diamonds). The impact of ETGs, coming from electron scales ($k_y\rho_s > 1$), on q_e increases with increasing R/L_{Te}. For R/L_{Ti}=5.77 it is negligible ($\sim 5\%$) at experimental R/L_{Te}=9, and remains moderate ($\sim 18\%$) at R/L_{Te}=14. For R/L_{Ti}=5.17, the ETG flux is 20% at R/L_{Te} =11, to be compared with the 10% of the R/L_{Ti}=5.77 case. So the ETG fraction is increasing at low R/L_{Ti}, but overall the q_e^{GB} and q_i^{GB} values are lower due to reduced ion-scale flux. These non-linear results are consistent with the simple linear criterion based on the $(\gamma/k_y)_{max,ETG}/(\gamma/k_y)_{max,ITG}$ ratio that has been used in Section 3.2 (Figure 4). In general it is evident that there is a conflict between the need of depressing the ion scales to enhance ETGs and explain the high q_e^{GB} points, and the need to still match the q_i^{GB} values and the lower q_e^{GB} part of the curve, which requires ion-scale flux. The spectra of the GENE nonlinear electron heat fluxes are shown in Figures 8 for the case R/L_{Ti}=5.77, comparing multi-scale and ion-scale results, for the extreme values of R/L_{Te}=9,14, indicated in blue and red, respectively. The agreement of ion- and multi-scale simulations is good on the ion-scales. The electron scales show a different 'shape' for the two R/L_{Te} values: while for the lower R/L_{Te} the ETG peak can be distinguished at large wavenumbers, for the larger R/L_{Te} a continuous TEM-ETG branch is present, making the ETG peak not distinguishable. This is consistent with the linear results, where two distinct ITG and ETG peaks can be distinguished looking at the growth rate spectrum for R/L_{Te}=9, which are replaced by an almost monotonically increasing TEM-ETG branch for R/L_{Te}=14 (see Figure 4). In Figure 9 the spectra of the GENE nonlinear electron heat fluxes are shown for R/L_{Te} =11 for the two cases R/L_{Ti}=5.17 and R/L_{Ti}=5.77. This shows the increase from 10% to 20% of the ETG heat flux fraction when lowering R/L_{Ti}.

On the basis of these results, we have to conclude that with the present choice of parameters the ETG flux predicted by the multi-scale simulation is not sufficient to explain the experimental q_e at R/L_{Te}=9 for the high flux points. Moreover, the deviation of the multi-scale R/L_{Te} stiffness from the TEM-driven ion-scale one is small. More sensitivity studies, varying parameters within uncertainties, particularly the impurity mix and their gradients, would be needed but are not feasible for lack of resources for further multi-scale simulations. In particular, we cannot exclude that cross-scale effects like the one observed in [3], consisting in a backward energy transfer from ETGs to ion scales when ion scales are marginally stable, could allow to simultaneously match electron and ion heat fluxes with multi-scale simulations, when further decreasing R/L_{Ti} closer to the ITG threshold, although we have never observed this kind of behaviour in the simulations carried out so far. However, due to the large ion stiffness, the search of an 'optimal' value of R/L_{Ti} would require a fine R/L_{Ti} scan of GK NL multi-scale simulations, which is beyond the available computational resources. This test is thus left for future work. In the following section we will try to use the quasi-linear TGLF model, which features ETG transport and multi-scale interactions, to further explore the sensitivity of the q_e^{GB} vs R/L_{Te} on Z_{eff} and the choice of impurity mix.

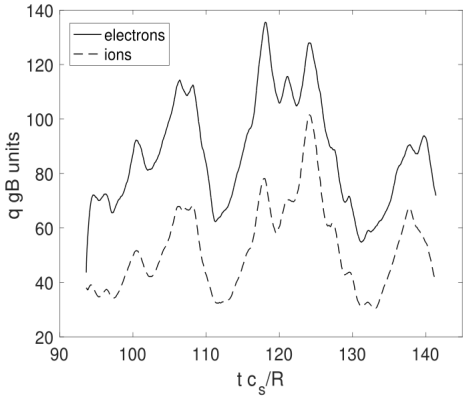

Figure 6. Time traces of the electron and ion heat fluxes in gB units for the GENE multi-scale simulation with R/L_{Te}=14.

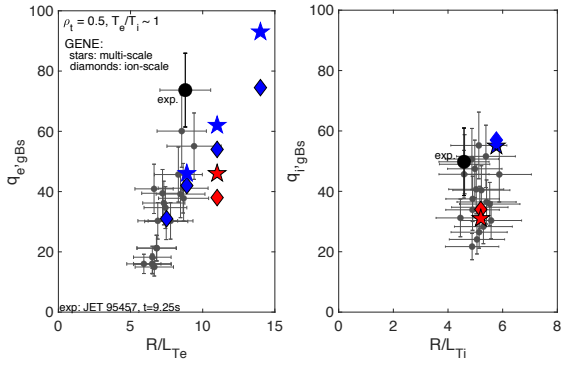

Figure 7. GENE nonlinear heat fluxes in gB units vs R/L_T, for electrons (left) and ions (right), comparing multi-scale (blue stars with R/L_{Ti}=5.77, red stars with R/L_{Ti}=5.17) with ion-scale (blue/red diamonds) runs. The experimental value (JET pulse #95457) is indicated by a large circle, while the small circles show the other experimental pulses with $T_e/T_i \sim 1$.

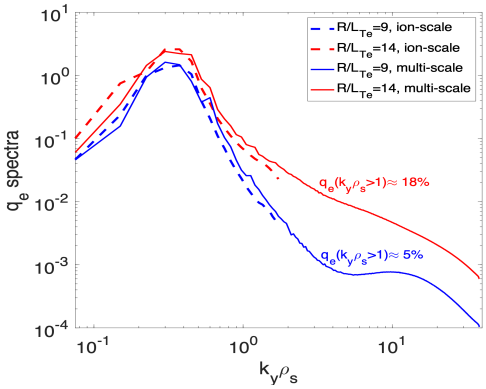

Figure 8. GENE nonlinear electron heat flux spectra for the extreme cases R/L_{Te}=9 (blue) and R/L_{Te}=14 (red), comparing ion-scale results (dashed) with multi-scale ones (solid) for the case R/L_{Ti}=5.77.

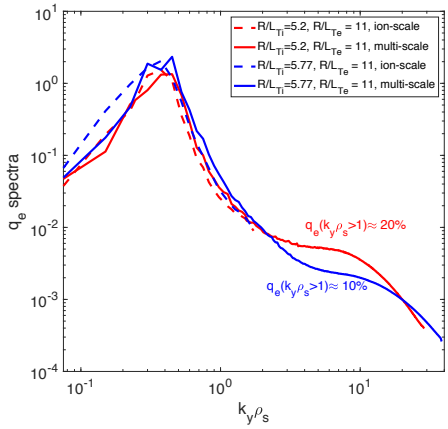

Figure 9. GENE nonlinear electron heat flux spectra for R/L_{Te}=11 for the cases R/L_{Ti}=5.17 (red) and R/L_{Ti}=5.77 (blue), comparing ion-scale results (dashed) with multi-scale ones (solid).

4. TGLF simulations

For the validation of TGLF against experimental data and GENE simulations the two most recent versions of TGLF have been used: a) TGLF SAT1-geo, released in November 2019 and featuring, with respect to the original TGLF SAT1 [11], an improved description of geometrical effects and calibration against CGYRO nonlinear simulations; b) TGLF SAT2, released in January 2021, featuring further improvements and better agreement with CGYRO as discussed in [12].

The TGLF model has been run in stand-alone mode at ρ_{tor} =0.5 for shot 95457 (t=9.3 s) with the same input parameters used for the GENE multi-scale simulation, in order to compare the electron stiffness to experiment and GENE results, and with different impurity combinations, to test the sensitivity to the impurity mix. We note that whilst the GENE runs were all run with general flux surface geometry, accounting for the up/down asymmetry of the JET shape, TGLF features an up/down symmetric Miller geometry approximation [25]. In addition, integrated modelling using the ASTRA code [18] has been performed for selected discharges of the various groups.

4.1 Stand-alone TGLF results

Figure 10 shows the comparison between the experimental data with T_e/T_i ~1, the GENE multi-scale simulations and the TGLF SAT1-geo and SAT2 simulations for shot 95457 at ρ_{tor} =0.5. The TGLF simulations use the same input parameters as GENE, with 3 species, Z_{eff}=1.5 and electromagnetic effects (B_{perp} fluctuations). However, the TGLF ion heat flux at the nominal R/L_{Ti} is significantly underestimated, so we also show the cases with increased R/L_{Ti} to match q_i^{GB}, which is key for a correct reproduction of multi-scale interactions. The electron stiffness of SAT1-geo in the TEM part of the curve is a bit lower than in experiment and in GENE multi-scale, but overall acceptable, whilst that of SAT2 is significantly underestimated. Both models feature an ETG wall at quite large values of R/L_{Te}, so that they miss reproducing the experimental uppermost points by a factor >2 in q_e^{GB}, as for the GENE multi-scale, which however does not feature such sharp ETG wall. As a matter of fact, the only case where the TGLF SAT1-geo curve approaches the experimental data also in the uppermost region is that with Z_{eff}=1, which however is experimentally unrealistic. Therefore, with the choice of parameters used in the multi-scale, we conclude that also TGLF cannot achieve a satisfactory reproduction of the upper part of the curve. At the radius of our analysis the fast ion population from ICRH and NBI is very small for shot 95457 (n_{fast}/n_e~2.5 10^{-3}) so they do not influence the results. However due to the strong sensitivity of the TGLF simulations to Z_{eff}, and given that previous GENE multi-scale simulations both in JET [4] and AUG [10,26] showing significant ETG contributions were in fact made with Z_{eff}=1 for lack of computational resources, we have studied in more detail with TGLF the effect of impurities for this JET case. The results are summarized in Figure 11. Here we compare the cases with the real mix of only light impurities (Be, C, Ne with Z_{eff}=1.3) at R/L_{Ti}=5.17 and R/L_{Ti}=5.77, the case with only Be at 2.5%, Z_{eff}=1.3, R/L_{Ti}=5.77 and the case with also the heavy impurities, Z_{eff}=1.7, R/L_{Ti}=5.77.

One can see that at least the case with the real mix of only light impurities with R/L_{Ti}=5.77 (blue circles) approaches the experimental data (both q_e and q_i), and this is an experimentally more relevant simulation than the Z_{eff}=1 case of Figure 10. Substituting these with only Be (red squares) has a worse effect – for same Z_{eff} – which suggests a complex role of impurities in determining the ETG component. Lowering R/L_{Ti} and R/L_n (green crossed squares) as expected brings more ETG fraction but lower ion-scale flux, so overall worse agreement with experiment. When including also heavy impurities (violet diamonds), which should be the real experimental case, the ETG component is quenched and the simulations depart from the experiment. This remains to be understood, with new multi-scale GK runs when resources will be available, in which the light and heavy impurities are treated separately, and not lumped together as in the multi-scale GK simulations presented in Sect.3.

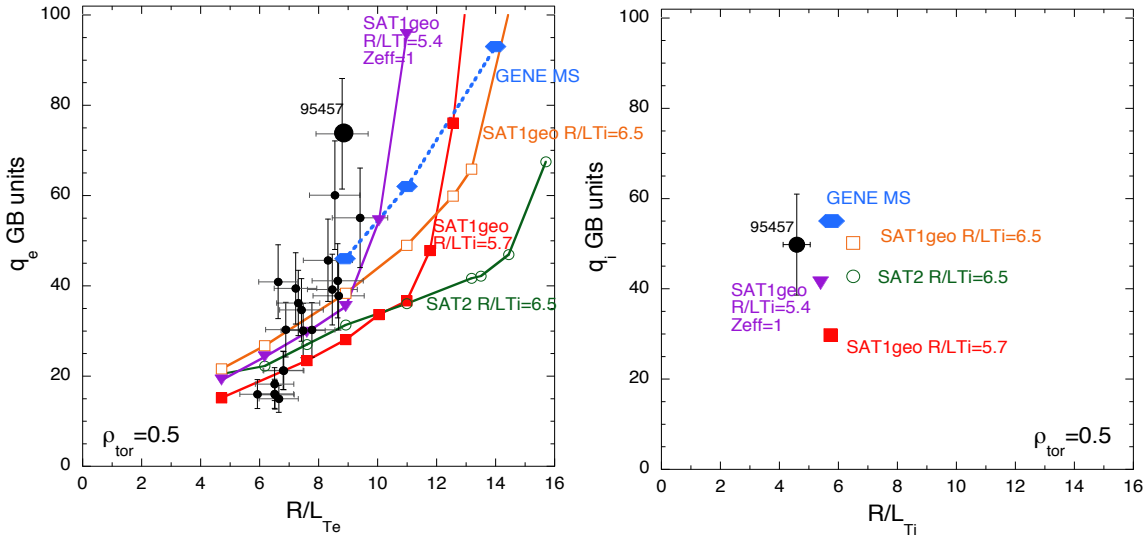

Figure 10. q_e^{GB} vs R/L_{Te} for the experimental set at T_e/T_i ~1 (black circles) and TGLF stand-alone simulations with same parameters as the multi-scale with R/L_{Ti}=5.77 (blue diamond), but with R/L_{Ti} also adjusted to 6.5 to match q_i^{GB}, as labeled in the figure. In the q_i^{GB} vs R/L_{Ti} figure only the simulated shot is reported for sake of clarity. The case with Z_{eff}=1 is also shown.

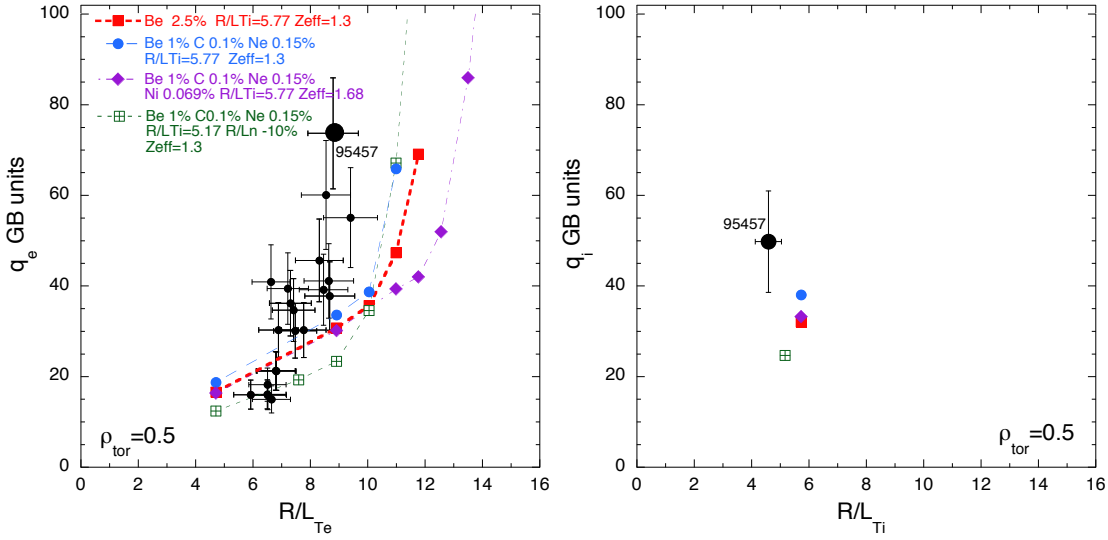

Figure 11. q_e^{GB} vs R/L_{Te} and q_i^{GB} vs R/L_{Ti} for the experimental set at T_e/T_i ~1 (black circles) and TGLF SAT1geo stand-alone simulations for various choices of impurities, as labelled in the legend. The case ⊞ has the same impurities as the case ● but reduced R/L_{Ti} and R/L_n.

4.2 TGLF profile simulations

Profile simulations of T_e, T_i and n_e have been made using the ASTRA code and the transport models TGLF SAT1-geo and SAT2. Rotation and safety factor have been used interpretatively and the impurity composition has been taken from the constrained multi-diagnostic analysis [23]. Typically one light impurity (Be, including also the contribution of Ne to Z_{eff}) and one heavy impurity (bundling Ni and W together) have been included in the simulation and used in TGLF as kinetic species, although they are not evolved but their density profile is taken proportional to the n_e profile. Fast ions cannot be included as kinetic species at the standard resolution used for integrated modeling, but their density is accounted for in calculating main ion dilution and their pressure is added to the thermal one to include their effects on equilibrium.

Figure 12 shows the TGLF SAT1-geo (left column) and TGLF SAT2 (right column) simulations for shot 95457 (the uppermost point of the T_e/T_i~1 set studied in detail in Sections 3 and 4.1). When predicting the 3 channels T_e, T_i and n_e (upper row), n_e is a bit over-predicted inside mid-radius, which gives origin to additional TEM electron heat transport. In spite of this, T_e is also over-predicted inside mid-radius, and even more so when n_e is assumed fixed from experiment (lower row). This is consistent with expectations from the stand-alone results of Figure 10, indicating large missing electron heat flux. T_i is instead well predicted. Using the TGLF SAT2 model worsen the situation, since as seen in Figure 10 it has lower stiffness than SAT1-geo. In fact in Figure 12 (right column) T_e appears even more overestimated (disregard the very central region where a strong mode appears, whose nature has not been investigated since this region

is not important for our ETG studies). These simulations confirm that some additional electron heat transport would be required to reproduce the experimental profiles, which could be ascribed to ETGs, but the model does not predict their appearance at the experimental R/L_{Te} but only at much higher R/L_{Te}, thereby failing to reproduce the experimental profiles.

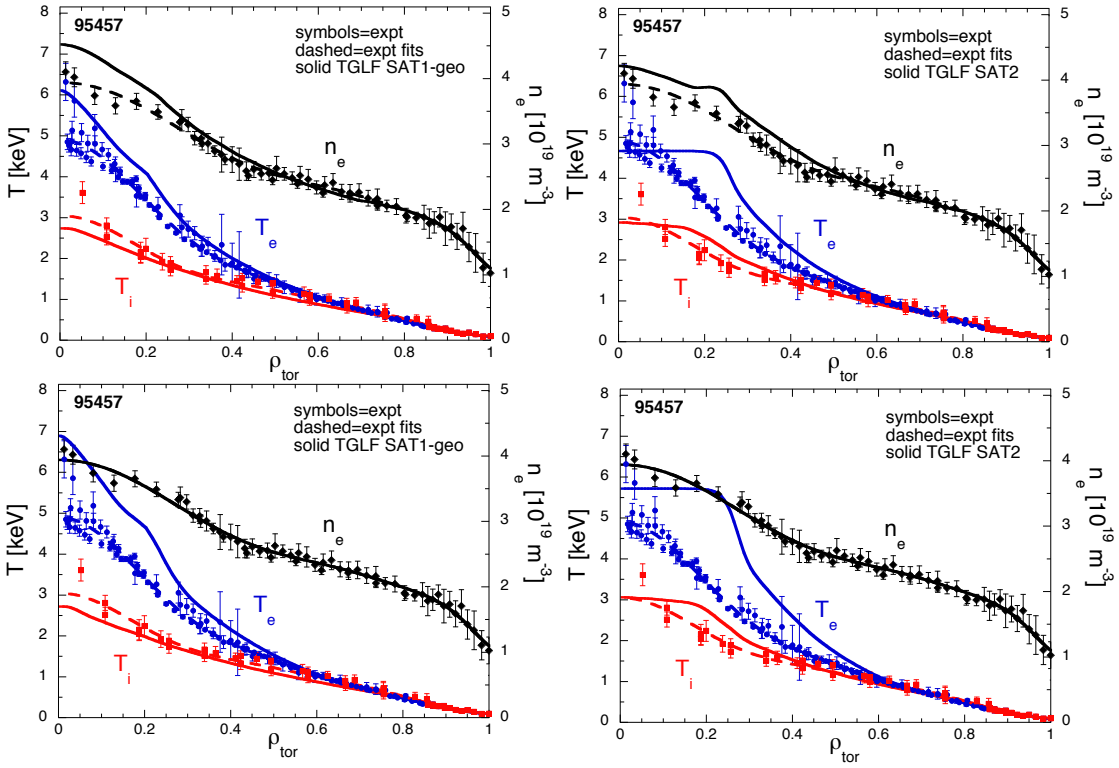

Figure 12. Profile simulations using TGLF SAT1-geo (left column) and SAT2 (right column) of shot 95457 at t=9.3s (P_{NBI}=0, P_{ICRH}=3 MW on-axis) with density predicted (upper row) and density held fixed to the experimental profile (lower row).

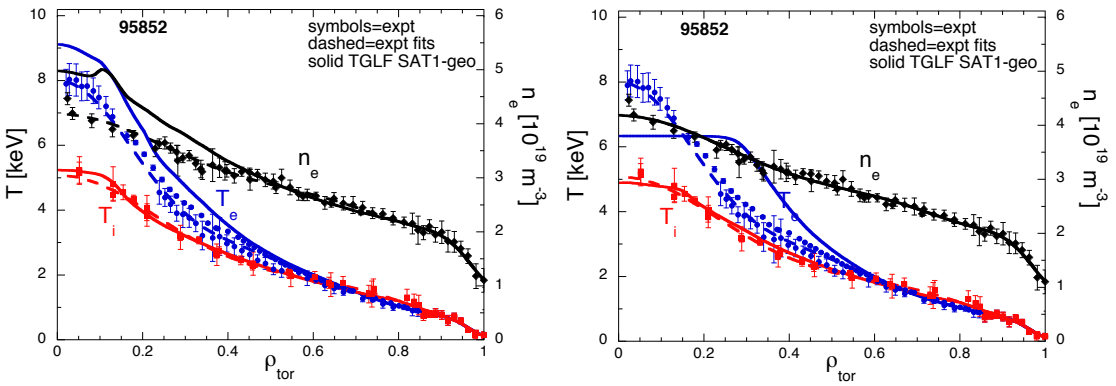

Figure 13. Profile simulations using TGLF SAT1-geo of shot 95852 at t=8 s (P_{NBI}=6.2 MW, P_{ICRH}=5.7 MW on-axis) with density predicted (left) and density held fixed to the experimental profile (right).

We now examine TGLF simulations for other 3 shots from Figure 3. This has been done only with SAT1-geo, given the worse performance of SAT2. First we examine 95852 at t=8 s, a shot of the same group T_e/T_i~1 but located a bit lower in q_e^{GB}. In Figure 13 one can observe qualitatively similar issues as for 95457, with T_e and n_e departing from experiment at an inner position, and T_i well predicted. For shot 95846 at t=10 s, belonging to the group of shots with T_e/T_i~1.3, we see in Figure 14 that n_e and T_i are very well predicted, and only T_e still shows some over-prediction. This group of shots, being relevant for the ITER PFPO-1 phase, has been addressed in detail together with similar ASDEX-Upgrade shots in a separate paper [27]. In these conditions where ETGs are expected to have a higher threshold, the TGLF model performs better in general, consistently with the observa-

tion in Figure 3 that this set of points maintains a milder stiffness level also in the upper part of the curve. Still, the TGLF electron stiffness remains slightly lower than the experimental one, resulting in some T_e overprediction for shots like 95846 which are at high q_e^{GB} , i.e. far from threshold. In fact, the only shots where TGLF performs really well are the high power ones, because in normalized flux they lie near threshold, so that only the linear physics of the threshold matters for the profile predictions. An example is shot 95460 at t=7.4 s (Figure 15), for which very good reproduction of all profiles is provided by TGLF.

In summary, regarding electron heat transport we can conclude that the TGLF SAT1-geo model can adequately describe plasmas that are near threshold (low q_e^{GB}), but it shows some under-prediction of electron stiffness level leading to T_e over-prediction, and in some cases also to n_e over-prediction. This is seen in spite of the fact that the model does feature ETG transport and multi-scale effects, which however appear to become important only at higher R/L_{Te} than in experiment.

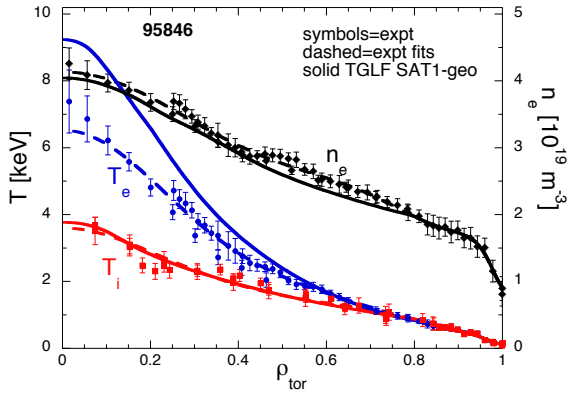

Figure 14. Profile simulations using TGLF SAT1-geo of shot 95846 at t=10 s (P_{NBI}=1.3 MW, P_{ICRH}=4.8 MW on-axis).

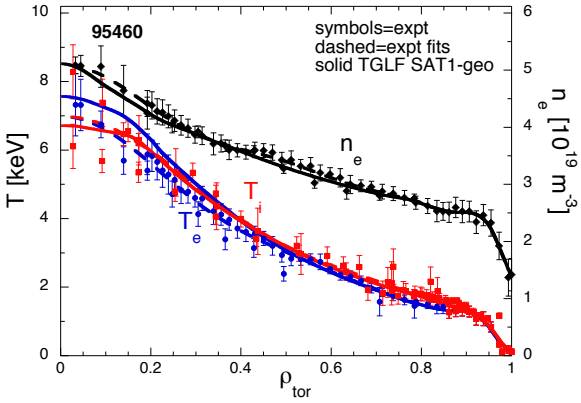

Figure 15. Profile simulations using TGLF SAT1-geo of shot 95460 at t=7.4 s (P_{NBI}=18.7 MW, P_{ICRH}=6.4 MW on-axis)..

6. Discussion and conclusions

A good set of experimental data with q_e scans at various T_e/T_i has been obtained on JET. It proved rather difficult to reach high values of q_e^{GB}, so the dataset includes very few points in the high q_e^{GB} region, which limits a conclusive assessment. Unfortunately T_e modulation was not feasible with ICRH in (H)-D scheme.

From the available data, we observe rather high electron stiffness in general, and particularly in the high q_e^{GB} region. We note that previous JET experiments using modulated ICRH in Mode Conversion scheme [4] also showed high electron stiffness, supporting the present results. The threshold R/L_{Te} does not show any clear dependence on T_e/T_i for this set of discharges. These two observations suggest a possible picture of ion-scale TEM/ITG responsible of q_e at low q_e^{GB} , with ETGs, if present, more likely to contribute to the high q_e^{GB} points. Therefore gyro-kinetic and quasi-linear simulations have been performed for the case with high q_e^{GB} to find out if theoretical predictions provide evidence of ETG flux.

Ion-scale GK simulations reproduce well the low q_e^{GB} region, but fail to get the high q_e^{GB} points. Increasing R/L_{Ti} or R/L_n within uncertainties can match the high q_e^{GB} point but without changing the slope, therefore producing mismatch at low q_e^{GB}. Under the assumption that the data are homogeneous in parameters, i.e that small differences between shots do not affect the average stiffness observed, we can then conclude that ion-scale GK simulations fail in reproducing the observed stiffness level and the high q_e^{GB} points.

Multi-scale GK simulations, with one impurity species bundling together light and heavy impurities, for R/L_{Ti}=5.77 (matching q_i^{GB} and q_e^{GB} at lower fluxes) do not show ETG flux at experimental R/L_{Te}=9, but only for R/L_{Te}>11, up to 20% at R/L_{Te}=14. If R/L_{Ti} is decreased to 5.17, the ETG fraction increases but the low k part of the flux decreases, overall underestimating the data even more. Both simulations then fail to explain the experimental cases. Sensitivity tests, particularly with different choices of impurities, would be needed but presently cannot be done with GK multi-scale simulations for lack of numerical resources.

TGLF was run stand-alone with same settings as the multi-scale GK simulations (and same single impurity) and shows a bit lower ion and electron stiffness than GK, particularly with the SAT2 saturation rule, which leads to the need of using higher R/L_{Ti} to match the q_i. A strong ETG wall appears for R/L_{Te} >12 for experimental Z_{eff}, whose position is strongly sensitive to Z_{eff}, but only approaches the experiment for Z_{eff}=1. Also the electron stiffness of the lower q_e^{GB} part is underestimated, and heavily by SAT2. When using the real mix of light impurities however, the TGLF SAT1geo simulations fall not far from experiments (both q_e and q_i). However adding the heavy impurities shifts again the ETG wall far from the experiment. These effects of impurities on ETG non-linear threshold and stiffness will then require further studies, as they are basically unexplored, both experimentally and theoretically. In Refs.[2-3] impurities are included in the multiscale simulations but their effect is not singled out. Profile simulations with TGLF using both light and heavy impurities in general overpredict T_e and in some cases also n_e. Good agreement is found only for high power cases near the TEM threshold, where a correct prediction of electron stiffness does not matter much for the resulting profile.

Concerning ITER relevance of these results, we have spanned a range of T_e/T_i that is useful both for ITER

PFPO-1 (the T_e/T_i ~1.3 set) and for ITER FPO (T_e/T_i ~1). The T_e/T_i ~0.9 set is more typical of ion heated machines like JET at high power. It has to be noted that the ITER FPO due to high temperatures and density will be at low q_e^{GB}, so more similar to our high power set close to threshold, where electron stiffness does not impact much. Still, it is not obvious without dedicated simulations to establish whether such threshold will be the TEM or the ETG one, and in particular the physics of multi-scale interactions setting the non-linear ETG threshold could be relevant in determining the ITER R/L_{Te}. Therefore it is important to validate the theoretical models in this respect on present devices. In fact, in TGLF simulations of the ITER FPO baseline scenario presented in [28], an ETG contribution up to 16% of q_e was predicted. Given that in the present study we found that TGLF may be underestimating the ETG flux, this certainly calls for further investigation. Regarding ITER PFPO-1 conditions, the validity of QL models has been studied in detail in [27] on AUG and JET shots. It was found that TGLF performs rather well for high/medium T_e/T_i, dominated by TEM, but there is a tendency to over-predict T_e when approaching T_e/T_i ~1. One of the JET shots used for this study in [27] is shown also in the present paper in Fig.14. This may hint to a possible ETG contribution also in these conditions.

In conclusion, the experimental hints of a possible ETG contribution to electron heat flux at high R/L_{Te} and T_e/T_i=1 do not seem supported by gyrokinetic multi-scale simulations, although the ion scale simulations do show a lack of electron heat flux driven by R/L_{Te}. Lack of numerical resources prevented an adequate sensitivity study with multiscale GK simulations. The use of TGLF for more affordable sensitivity studies indicates a strong sensitivity of ETGs to the impurity mix and Z_{eff}, with reasonable agreement with experiment being reached only neglecting the heavy impurities. This calls for further investigations. Given the scarceness of the dataset in the high q_e^{GB} region, new experimental data from JET in different conditions as well as from other devices that can add T_e modulation information and/or measurements of turbulence at the electron scales may provide in the future additional insight into this difficult topic A key ingredient will be as well an improvement of high power computing speed, allowing a more handy use of gyrokinetic codes for a proper sensitivity study with multiscale simulations. This may eventually lead to a final assessment of the role of ETG transport in present and future machines.

Acknowledgments

This work has been carried out within the framework of the EUROfusion Consortium and has received funding from the Euratom research and training programme 2014-2018 and 2019–2020 under grant agreement No. 633053. The views and opinions expressed herein do not necessarily reflect those of the European Commission. We acknowledge fruitful discussions with C.Angioni, J.Citrin and T.Goerler. The gyrokinetic simulations were performed on CINECA Marconi HPC within the projects MULTJET and WPJET1. This work was also conducted under the auspices of the ITPA Topical Group on Transport &Confinement.

References

[1] Ryter F. *et al* 2006 *Plasma Phys. Control. Fusion* **48** B453
[2] Howard N T *et al* 2013 *Nucl. Fusion* **53** 123011
[3] Howard N T *et al* 2016 *Nucl. Fusion* **56** 014004
[4] Bonanomi N *et al* 2018 *Nucl. Fusion* **58** 124003
[5] Smith S P *et al* 2015 *Nucl. Fusion* **55** 083011
[6] Mariani A *et al* 2019 *Nucl. Fusion* **59** 126017
[7] Ryter F *et al* 2019 *Nucl. Fusion* **59** 096052
[8] Jenko F *et al* 2001 *Phys. Plasmas* **8** 4096
[9] Maeyama S *et al* 2015 *Phys. Rev. Lett*. **114** 255002
[10] Bonanomi N *et al* to be submitted
[11] Staebler G M *et al* 2016 *Physics of Plasmas* **23** 062518
[12] Staebler G M *et al* 2021 *Plasma Phys. Control. Fusion* **63** 015013
[13] Brix M. et al 2008 *Rev. Sci. Instrum*. **79** 10F325
[14] Ho A *et al*, 2019 *Nucl. Fusion* **59** 056007
[15] Challis C. *et al* 1989 *Nucl. Fusion* **29** 563
[16] Eriksson L.-G., Hellsten T. and Willén U. 1993 *Nucl. Fusion* **33** 1037
[17] Hedin J. et al 2002 *Nucl. Fusion* **42** 527
[18] Pereverzev G.V. and Yushmanov P.N. 2002 Technical Report IPP 5/98, Max-Planck-Institut fur Plasmaphysik, Garching (https://pure.mpg.de/rest/items/item_2138238/component/file_2138237/content)
[19] Peeters A.G., Angioni C., Apostoliceanu M., Jenko F., Ryter F. and The ASDEX Upgrade Team 2005 *Phys. Plasmas* **12** 022505
[20] Jenko F., Dorland W., Kotschenreuther M. and Rogers B.N. 2000 *Phys. Plasmas* **7** 1904
[21] Görler T., Lapillonne X., Brunner S., Dannert T., Jenko F., Merz F., and Told D. 2011 *J. Comput. Phys*. **230** 7053
[22] Brizard A.J., and Hahm T.S. 2007 *Rev. Mod. Phys*. **79** 421
[23] Sertoli M. *et al* 2019 *Journal of Plasma Physics* **85** 905850504.
[24] Staebler G.M., Howard N.T., Candy J., and Holland C. 2017 *Nucl. Fusion* **57** 066046
[25] Miller R.L., Chu M.S., Greene J.M., Lin-Liu Y.R., and Waltz R.E. 1998 *Phys. Plasmas* **5** 973
[26] Mariani A.et al, invited talk at AAPPS (online) October 2020
[27] Kiefer C.K. *et al*., Validation of quasi-linear turbulent transport models against plasmas with dominant electron heating for the prediction of ITER PFPO-1 plasmas, accepted for publication in Nucl.Fusion.
[28] Mantica P. *et al*., 2020 *Plasma Phys. Control. Fusion* **62** 14021